

Research Article

Open Access

Kumar Sankaran, Partheban Manoharan, Sofana Reka S, Santanu Chattopadhyay *

A brief insight into the prediction of water vapor transmissibility in highly impermeable hybrid nanocomposites based on bromobutyl/epichlorohydrin rubber blends

<https://doi.org/10.1515/chem-2018-0124>

received August 31, 2017; accepted May 7, 2018.

Abstract: The present work proposes a schematic model for predicting the water vapor transmissibility in hybrid nanocomposites based on bromobutyl (BIIR)/epichlorohydrin (CO) rubber blends. Morphology study reveals the exfoliation of nanoclay and development of hybrid nanostructures in the rubber nanocomposites. A unique correlation between water vapor transmissibility and gas (oxygen) permeability through the rubber nanocomposites has been systematically derived. The prediction of relative water vapor transmissibility was achieved by considering the polar path along with the existing tortuous path and has been validated. Interestingly, it is found that the water vapor transmissibility (T_w) directly depends on the weight fraction of the polar rubber (Φ_p) in the rubber blend and permeability to gas (P_g) of the nanocomposites.

Keywords: Nanostructure morphology; water vapor transmissibility; modeling of transmissibility; gas permeability; surface hydrophilicity.

1 Introduction

Barrier properties are the prime requisite for rubber membranes, bladders, tubes, and tubeless tires. A low barrier property significantly affects the performance and durability of the rubber product. In particular, the

water vapor transport potentially causes degradation mechanism like hydrolysis and corrosion affecting the electrical conductivity and mechanical properties of the composites considerably [1]. Water vapor barrier is of significant value for tire inner liner material as it prevents the liner material from corroding steel belts and bead wires. It also increases the adhesion strength with ply compounds. It is, therefore, important to analyze the water vapor transmission characteristics and to develop a highly impermeable rubber compound. Diffusion and permeation of gas and vapors in rubbers were briefly discussed in earlier literature [2-5]. However, modeling, theoretical prediction, and the correlation between water vapor transmissibility and gas permeability in the rubber nanocomposites were hardly found in literature and needs exploration.

Layered silicates due to their high aspect ratio and platelet like structure, offers low permeability in the nanocomposites. The dispersion of the nanoclay is the key factor in reinforcing the rubber and to improve the properties of the rubber nanocomposites. BIIR (bromobutyl) is the most favored rubber for the construction of tire inner liners, heat resistant tubes, bladders and pharmaceutical ware due to lower permeability to gases [6]. Polyepichlorohydrin rubber (CO) also offers excellent resistance to gas permeability [7], which is even lower than that of the butyl rubber. Frank et al. claimed that blending of epichlorohydrin rubber with brominated butyl rubber and having delaminated talc in the rubber composite has lower air permeability [8]. It finds potential application in tire inner liners with low permeability. Hence, CO rubber is suitably blended with BIIR in order to further reduce the permeability of the rubber nanocomposites.

This present work discusses in detail the effect of the polar fraction of rubber blends, and nanoclay, on the permeation characteristics of the unique BIIR-CO hybrid nanocomposites. A unique schematic has been modelled to determine the relative moisture transmissibility. An

*Corresponding author: Santanu Chattopadhyay, Rubber Technology Centre, Indian Institute of Technology, Kharagpur-721302, India, E-mail: santanu@rtc.iitkgp.ernet.in
Kumar Sankaran, Partheban Manoharan: Rubber Technology Centre, Indian Institute of Technology, Kharagpur-721302, India
Sofana Reka S: VIT University, Chennai Campus, Tamilnadu, India

Table 1: Compound formulation^a (all ingredients are measured in phr, parts per 100 g of rubber).

| Chemical Ingredients | B ₁₀₀ H ₀ CB ₅₀ NC ₀ | B ₁₀₀ H ₀ CB ₅₀ NC ₅ | B ₉₀ H ₁₀ CB ₅₀ NC ₅ | B ₈₀ H ₂₀ CB ₅₀ NC ₅ |
|---------------------------|--|--|--|--|
| BIIR 2255 | 100 | 100 | 90 | 80 |
| Hydrin H-55 | - | 0 | 10 | 20 |
| Stearic Acid | 2 | - | - | - |
| Calcium stearate | - | 1.5 | 1.5 | 1.5 |
| Process Promoter | 15 | 15 | 15 | 15 |
| Cl Resin | 2 | 2 | 2 | 2 |
| CB N 660 | 50 | 50 | 50 | 50 |
| Cloisite 20A | - | 5 | 5 | 5 |
| Zisnet F-PT | - | - | 0.2 | 0.2 |
| Cure Package ^b | 4.8 | 4.8 | 4.8 | 4.8 |

^aCompound designation B-BIIR, H-CO, CB- Carbon black, and NC-Cloisite 20A. Subscripts indicate the respective dosage level in phr

^bCure package consists of zinc oxide (ZnO), 2,2'-dithiobis(benzothiazole) (MBTS), Sulphur, and N-(cyclohexylthio)phthalimide (CTP/PVI).

equation has been derived based on the model to correlate water vapor transmissibility with the gas permeability of the nanocomposite.

2 Experimental

2.1 Materials

Hydrin H 55 (specific gravity of 1.37), which is a homopolymer of epichlorohydrin (CO) and Zisnet F-PT (2,4,6 trimercapto-sym-triazine) chemical was kindly provided by M/S Zeon Chemicals, Louisville KY. Bromobutyl rubber (BIIR-2255) was purchased from M/S Exxon Mobil. The organically modified montmorillonite (OMMT) nanoclay (Cloisite 20A) was purchased from M/S Southern Clay Products Inc. Gonzales TX. Carbon black (GPF N 660 grade) was procured from M/S Philips Carbon Black Limited (PCBL), India. Nytex 810 (Naphthenic oil) was supplied by M/S Nynas. Span-60, an anti mill-sticking agent, was procured from M/S Sigma-Aldrich, USA. Other chemicals were supplied by the local vendors.

2.2 Preparation of rubber blend nanocomposites

Rubber nanocomposites were mixed in an internal mixer, Brabender Plasticorder. Mixing was performed in two stages for achieving better dispersion of nanoclay in the rubber matrix. The first stage mixing (master batch)

includes melt mixing of BIIR rubber and pre-blended CO-Zisnet F-PT stock, followed by the addition of nanoclay, process aids, carbon black, oil and other functional additives. Nanoclay was added at the beginning of the mix to have better dispersion in the rubber matrix. The addition of the curing agent and accelerators in the second stage mixing constituted the final batch. Compounding temperature was set at 55°C and the rotor speed was maintained around 50 rpm. The total mixing time of the rubber nanocomposites was 10 minutes. Cure characteristics of the samples were obtained by using an oscillating disc rheometer (ODR, Monsanto Rheometer 100) equipped with a digital thermologger operated at 170°C. The samples were cured for characterization based on the optimum cure time (OCT) obtained from ODR. Compound formulations are listed in Table 1. B₁₀₀H₀CB₅₀NC₀ is the standard BIIR compound. The effect of nanoclay is analyzed in B₁₀₀H₀CB₅₀NC₅. The combined effect of polar fraction and nanoclay is analyzed in B₉₀H₁₀CB₅₀NC₅ and the effect of an increase in the polar weight fraction is studied in B₈₀H₂₀CB₅₀NC₅.

3 Characterization

Structural analysis of nanofillers and rubber vulcanizates with different dosages of nanoplatelets were determined by X-ray diffraction (XRD, X-PERT PRO) using Cu anode target ($\lambda = 0.154$ nm) with a scan step size of 0.02 °. The d-spacing of nanoplatelets was calculated using the Bragg's law and structural aspects (intercalation or exfoliation) of the nanoplatelets in the rubber matrix were

determined from the peak intensities. The samples were placed vertically in front of the X-ray source. The detector was allowed to move at an angle of 2θ , while the sample was allowed to move at an angle θ , to pick up the diffracted rays by the detector.

The samples for high-resolution transmission electron microscopy (HRTEM) analysis were carefully made by ultra cryo-microtome using a Leica ultracut. Since the samples were elastomeric in nature, ultramicrotome was performed below the glass transition temperature of the blended rubbers ($-75\pm 5^\circ\text{C}$) using sharpened glass knives with a cutting edge of 45° . Dispersion of nanoclay in the nanocomposites was extensively analyzed by using HRTEM. The cryotomed sections were supported on a copper grid for capturing photomicrographs. The microscopy was performed using JEM-2100, JEOL, Japan.

Blend compatibility of the rubber blends were analyzed by dynamic mechanical analyzer (DMA) using Metravib 50 N, France, using tension mode. The samples were subjected to sinusoidal displacements with varying temperature sweeps (-100 to $+80^\circ\text{C}$) at a frequency of 10 Hz and a strain of 0.15%. Tan delta was measured for each sample in above mentioned temperature sweep.

Oxygen has been used as the test gas throughout the permeability experiment and is referred as gas permeability. Gas permeability of the nanocomposites was measured following GB 1038 standard using Labthink permeability tester at $40\pm 1^\circ\text{C}$. By measuring the pressure differences, the gas transmission rate (GTR) of the specimen was measured, and average values are reported.

Water vapor transmissibility was determined on a thin sheet (1mm thickness) using WVTR SG 3/33, MOCON, USA referring ASTM F 1249-06 at temperature around $40\pm 0.5^\circ\text{C}$ and RH $90\pm 3\%$.

Surface hydrophilicity/hydrophobicity was measured using water droplet with Rame-Hart standard goniometer (Model 260, F4 series, USA) using Dropimage Advanced V2.7 software.

Ethical approval: The conducted research is not related to either human or animals use.

4 Results and Discussion

4.1 Determination of nanostructural morphology

Morphology of the nanocomposites has been analyzed using XRD and TEM measurements. XRD spectra of the OMMT clay and BIIR-CO nanocomposites are shown in

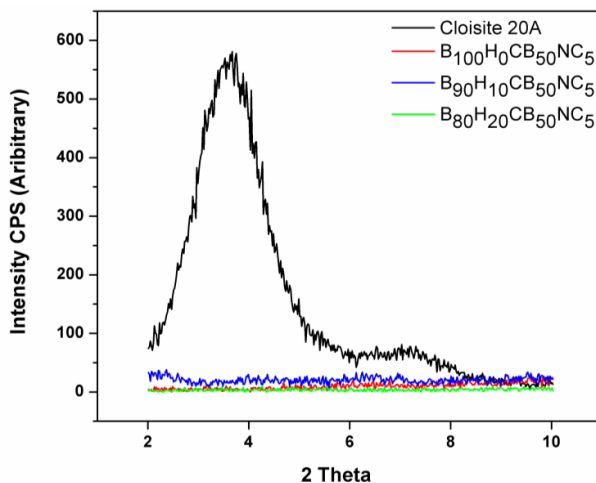


Figure 1: XRD reveals complete exfoliation of the nanoclay in the rubber nanocomposites.

Figure 1. The XRD of OMMT clay exhibits a sharp peak (001) at around $2\theta = 3.67$ (d-spacing of around 2.406 nm) but the nanocomposites, housing 5 phr of OMMT clay, do not display any sharp peaks over the entire range of 2θ studied. The pattern of the diffractogram is similar to all the samples revealing exfoliated state of dispersion of nanoclay in the rubber matrix. XRD analysis discusses the gallery spacing of the nanoclay. However, it is not a useful tool to understand the spatial distribution and structural heterogeneities of the nanoclay in the rubber matrix.

Dispersion of the nanoclay and the formation of hybrid nanostructures in the rubber nanocomposite are analyzed by using HRTEM. All the nanocomposites display a good level of dispersion of nanoclay in the rubber matrix. The nanocomposites also exhibit the formation of hybrid nanostructures with the development of nanounit and halo. The bending of the nanoclay around the carbon black particle (yellow dotted circle in Fig 2(a-c)) reveals the signature of 'nano unit' whereas the entrapment of nanoclay within the black particles corresponds to the halo (red circle in Fig 2(a-c)). The development of those hybrid nanostructures (NC-CB) and good dispersion of nanoclay channels the overall improvement in the filler connectivity as well as the properties of the nanocomposites [9-11].

4.2 Water vapor transmissibility

The diffusion coefficient of the water vapor in nanocomposites significantly contributes to its permeation path. A water vapor transmissibility model has been developed, which significantly explains the

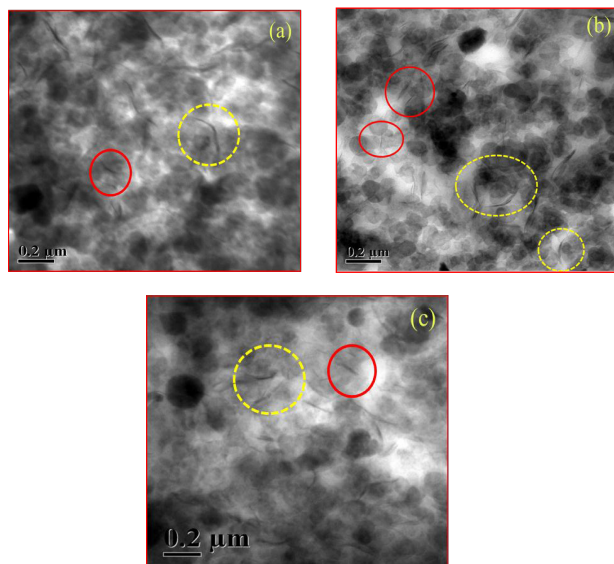


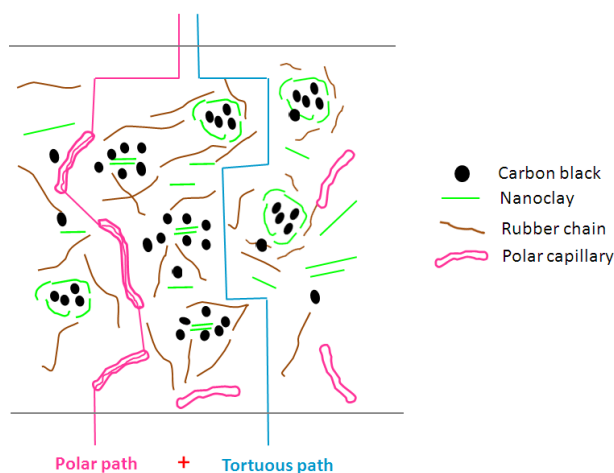
Figure 2: TEM Photomicrographs confirms development of hybrid nanostructures in the nanocomposites (a) $B_{100}H_0CB_{50}NC_5$ (b) $B_{90}H_{10}CB_{50}NC_5$ (c) $B_{80}H_{20}CB_{50}NC_5$.

possible paths of the diffusion of water vapor in the nanocomposites based on rubber blends.

4.2.1 The Model

The gas barrier of the nanocomposite corresponds to the tortuous path offered by the layered clay platelets [12]. The diffusion rate of the water vapor is relatively more than that of the gas molecule (O_2) due to the lower kinetic diameter of the water molecule [13,14]. However, the process of restriction to diffusion due to the tortuosity remains the same irrespective of the size of the gas molecule in the rubber nanocomposites. To understand the effect of the polar component on vapor transmissibility in the rubber nanocomposites, different ratios of rubber blends were mixed. The water vapor transmissibility in the rubber nanocomposite depends on the tortuous path and the polar tunnels. The tortuous path in the nanocomposite corresponds to the presence of nanoclay in the rubber matrix. The polar capillary corroborates the polar nature of the rubber blend nanocomposites. The two paths which possibly occur in the water vapor transmission process are schematically presented in Scheme 1. Tortuous route occurs due to the formation of nanoclay induced hybrid nanostructures. The polar route constitutes through the polar capillary of the rubber.

The polar chains act as a capillary, absorbing the vapor molecules. The effect is more pronounced if the



Scheme 1: A schematic model explaining plausible water vapor transmissibility mechanism in the rubber nanocomposite.

polar fraction is more as many such capillaries arise. The formation of polar tunnels can be better explained by understanding the effect of CO domain in BIIR-CO rubber blends (Figure 3). Typically, the nanocomposites based on BIIR-CO blends were analyzed. It is noted that an increase in the addition of CO rubber ($B_{80}H_{20}CB_{50}NC_5$) clearly displays two peaks at around -30°C and -9°C . It corresponds to the glass transition temperature of BIIR and CO respectively. This confirms that the higher dosage of CO rubber predominantly phase separate the BIIR-CO blend in the nanocomposite. However, the effect is minimal for the rubber blend having a lower dosage of CO rubber ($B_{90}H_{10}CB_{50}NC_5$). The influential presence of CO domain in the BIIR-CO rubber blend, therefore, essentially corroborates the existence of polar pathways or capillaries in the hybrid nanocomposite. Hence, the water vapor transmission is considerably dependent on the volume fraction of the clay and the weight fraction of polar rubber in the rubber blend nanocomposite.

4.2.2 Analysis of water vapor transmissibility in the rubber nanocomposite

From the above figure, the prediction of water vapor transmissibility in the rubber nanocomposites can be evaluated. Figure 4 depicts the variation of water vapor transmissibility and gas permeability with an increase in the polar fraction of the rubber blend nanocomposites. From the figure, it is observed that the gas permeability of the nanocomposites decreases as the weight fraction of the polar rubber increases. The formation of hybrid nanostructures also contributes to a significant reduction

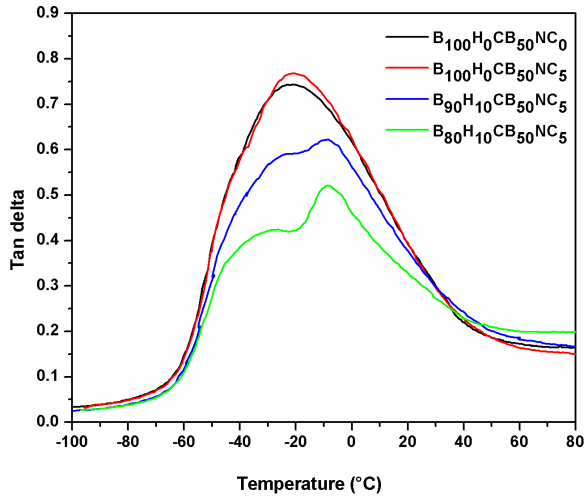


Figure 3: Loss factor (tan delta) as a function of temperature for the nanocomposites.

in the gas permeability in the rubber nanocomposites (see bottom inset in Figure 4). It is also clear that the water vapor transmissibility significantly changes with the weight fraction of the polar rubber and tortuosity offered by clay platelets. Water vapor transmissibility in the rubber nanocomposites is directly proportional to the polar fraction and permeability to gas. It can be obtained by using the following equation:

$$T_w \propto (\Phi_p) (P_c) \quad (1)$$

Where T_w represents water vapor transmissibility, Φ_p is the weight fraction of the polar rubber in the rubber blend, and P_c is the permeability to gas of the rubber blend nanocomposites.

The figure depicts some interesting water vapor permeation characteristics which can be explained as follows:

(i) The water vapor transmissibility is predominantly dependent upon the permeability of the gas molecule for the non-polar rubber blend nanocomposites ($B_{100}H_0CB_{50}NC_5$). It is dependent only on the tortuous path offered by the clay platelets as there is no polar path. Therefore, the above equation can be written as follows:

$$T_w \propto P_c \quad (2)$$

(ii) There is a crossover point at $B_{90}H_{10}CB_{50}NC_5$. At this point, T_w is dependent on weight fraction of the

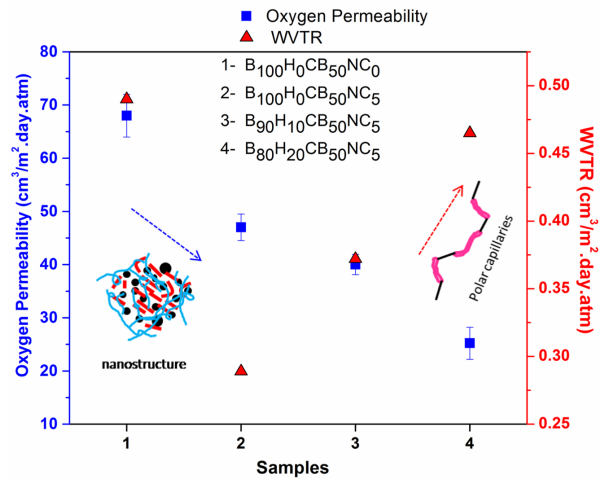


Figure 4: A Comparison of water vapor transmissibility and oxygen permeability with an increase in the polar weight fraction of the samples. Top inset: Formation of polar capillaries increases water vapor transmissibility (Polar path). Bottom inset: Formation of hybrid nanostructures decreases gas permeability (Tortuous path).

polar constituent as well as the permeability of the nanocomposites. In this case, equation 1 holds good.

$$T_w \propto (\Phi_p) (P_c) \quad (1)$$

(iii) After the cross-over point, the water vapor transmissibility shoots up in the nanocomposite $B_{80}H_{20}CB_{50}NC_5$. It signifies that T_w is predominantly dependent on polar weight fraction of the nanocomposite after the crossover point (see top inset of Figure 4).

$$T_w \propto \Phi_p \quad (3)$$

(iv) Hence for non-polar rubber blend nanocomposites, T_w is dependent on permeability (P_c), whereas, for polar rich rubber blend nanocomposites, T_w is dependent on polar weight fraction (Φ_p) of the rubber blends predominantly.

4.2.3 Prediction of relative water vapor transmissibility

From the schematic model and subsequent equations, the relative water vapor transmissibility in the rubber blend nanocomposites can be predicted. It is derived considering the relative gas permeability accounting to the tortuous path as well as the polar factor or polar component. The relative water vapor transmissibility (R_{WT}) in a rubber blend nanocomposites can be given as:

Table 2: Comparison of relative water vapor transmissibility obtained from model and experimental data.

| Compound | R_{WT} | |
|---------------------------|-------------|--------------|
| | Theoretical | Experimental |
| $B_{100}H_0CB_{50}NC_5$ | 0.70 | 0.59 |
| $B_{90}H_{10}CB_{50}NC_5$ | 0.78 | 0.76 |
| $B_{80}H_{20}CB_{50}NC_5$ | 0.98 | 0.95 |

$$R_{WT} = k \times R_{GP} \quad (4)$$

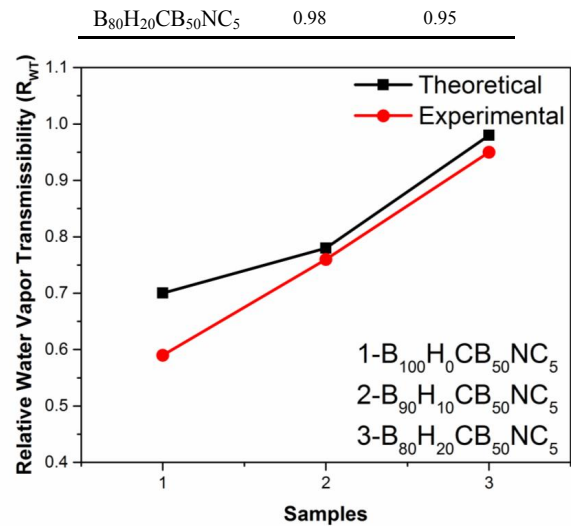
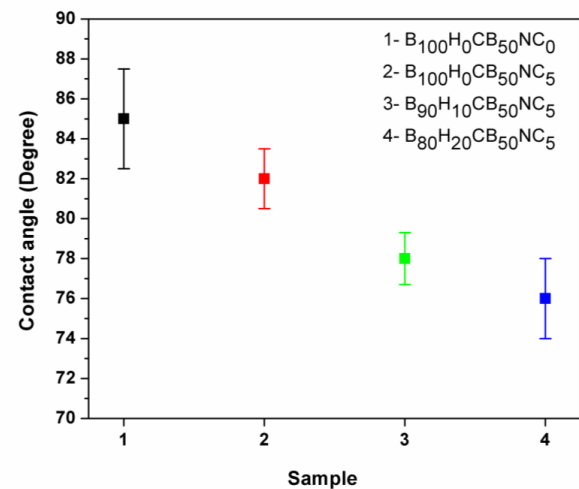
Where k is the polar component and R_{GP} is the relative gas permeability of the rubber nanocomposite, considering Bharadwaj model [12] for clay platelets. The polar component is determined using the following equation:

$$k = P_F \times \Phi_p \quad (5)$$

Where P_F is the polar factor and Φ_p is the weight fraction of the polar rubber in the rubber blend. The polar factor is due to the polar surface formed by the polar component of a molecule (<http://www.chemicalize.org/structure/#!mol=epichlorohydrin>). The polar factor is a good indicator of the water transport properties of the material. The polar factor (P_F) of epichlorohydrin rubber is around 12.53. As the polar factor decreases, k decreases and this polar effect is not considered for non-polar rubber blend nanocomposites $B_{100}H_0CB_{50}NC_5$, as mentioned in equation 2. The weight fraction (Φ_p) of the polar rubber (CO) in the rubber blend for $B_{90}H_{10}CB_{50}NC_5$ and $B_{80}H_{20}CB_{50}NC_5$ is 0.1 and 0.2 respectively. The relative gas permeability (R_{GP}) is theoretically determined using Bharadwaj equation [12] as follows,

$$R_{GP} = P_c/P_p = (1-\Phi) / [1+ (\alpha\Phi (2S+1))] \quad (6)$$

Where P_c and P_p represent the gas permeability of nanocomposite and neat polymer respectively, Φ is the volume fraction of nanoclay, α is the aspect ratio, and S is the order parameter. The theoretical prediction of the relative water vapor transmissibility is compared against the experimental data. The relative water vapor transmissibility values have been tabulated in Table 1, and the comparison between theoretical values and experimental data is shown in Figure 5. The theoretical calculations are done by employing the equations (4), (5), and (6). Experimental values are determined directly from the permeability tester.

**Figure 5:** Comparison of theoretical relative water vapor transmissibility against the experimental data of the samples.**Figure 6:** Surface hydrophilicity of the samples using contact angle measurement.

From the Figure 5, it is noticed that the theoretical values fit close with the experimental data for the rubber blend nanocomposites with the polar constituent. The relative water vapor transmissibility of the nanocomposites increases as the polar constituent increases. It signifies the impact of the polar fraction on water vapor transmissibility in the rubber blend nanocomposites.

4.3 Surface hydrophilicity analysis

The surface hydrophilicity of the samples is analyzed using contact angle measurements and is shown in Figure

6. The water droplet is used to determine the hydrophilicity or hydrophobicity of a surface. The surface is said to be hydrophilic if interaction force between water and surface is greater than that of the cohesive force associated with water droplet [16]. The surface is hydrophilic if the contact angle is below 90° and hydrophobic if it is above 90° .

It is noticed that $B_{100}H_0CB_{50}NC_0$ composite tends to be hydrophobic, and all nanocomposites exhibit surface hydrophilicity. $B_{100}H_0CB_{50}NC_5$ nanocomposite displays a marginal hydrophilic nature due to the presence of the nanoclay. The contact angles for all other samples remain well below 90° . The surface tends to be more hydrophilic with an increase in the polar nature of the rubber. It invokes that the water molecules are potentially imbibed towards the polar chain of the rubber.

5 Conclusions

The nanocomposites are prepared using melt compounding techniques. TEM photomicrograph confirms well-dispersed nanoclay within the blend matrix and the formation of hybrid nanostructures in the nanocomposites. The development of hybrid nanostructures considerably increases the barrier properties of the rubber nanocomposites. A successful attempt has been made to predict the water vapor transmissibility in a rubber nanocomposite using a schematic model. The relative water vapor transmissibility, derived theoretically, is compared and found to fit the experimental data. Thus, it signifies the dependency of the water vapor transmission characteristics on the polar fraction of the composites in addition to the tortuous permeation offered by the nanoclay platelets. Surface hydrophilicity of the nanocomposites confirms the same.

Acknowledgements: The authors acknowledge gratefully the management of CEAT LIMITED, Vadodara for funding this work. Special thanks to Mr.C.Cable (Zeon Chemicals, USA) for supplying free samples of CO rubber and Zisnet F-PT chemicals in this work.

Conflict of interest: Authors state no conflict of interest.

References

[1] Lutz B., Guan Z., Wang L., Zhang F., Lü Z., Water absorption and water vapor permeation characteristics of HTV silicone rubber material, In: 2012 IEEE International Symposium on

Electrical Insulation (10-13 June 2012, San Juan, PR, USA), IEEE Piscataway, 2012, 478-482.

- [2] Freeman B., Yampolskii Y., Pinnau I., Materials science of membranes for gas and vapor separation, John Wiley & Sons, 2006.
- [3] Barrer R.M., Chio H.T., In Solution and diffusion of gases and vapors in silicone rubber membranes, J. Polym. Sci., Part C: Polym. Symp., 1965, 111-138.
- [4] Long F.A., Thompson L.J., Diffusion of water vapor in polymers, J. Polym. Sci., 1955, 15, 413-426.
- [5] Johnson T., Thomas S., Natural rubber/epoxidised natural rubber-25 blends: morphology, transport phenomena and mechanical properties, J. Mater. Sci., 1999, 34, 3221-3239.
- [6] Thomas S., Ranimol S., Rubber Nanocomposites: Preparation, Properties and Applications, John Wiley: Singapore, 2010.
- [7] Cable C., Polyepichlorohydrin elastomers, Zeon chemicals L.P, Louisville, K.Y, USA, 2005.
- [8] Frank U.E., Frantzen A., Schweitzer C., Tire with innerliner containing talc and epichlorohydrin rubber, U.S Patent US 8,397,776 B2, 2013.
- [9] Konishi Y., Cakmak M., Nanoparticle induced network self-assembly in polymer-carbon black composites, Polymer, 2006, 47, 5371-5391.
- [10] Praveen S., Chattopadhyay P., Albert P., Dalvi V., Chakraborty B., Chattopadhyay S., Synergistic effect of carbon black and nanoclay fillers in styrene butadiene rubber matrix: development of dual structure, Compos. Part A Appl. Sci. Manuf., 2009, 40, 309-316.
- [11] Etika K.C., Liu L., Hess L.A., Grunlan J.C., The influence of synergistic stabilization of carbon black and clay on the electrical and mechanical properties of epoxy composites, Carbon, 2009, 47, 3128-3136.
- [12] Bharadwaj RK., Modeling the barrier properties of polymer-layered silicate nanocomposites, Macromolecules, 2001, 34, 9189-9192.
- [13] Van Amerongen G., Influence of structure of elastomers on their permeability to gases, J. Polym. Sci., 1950, 5, 307-332.
- [14] Sankaran K., Manoharan P., Chattopadhyay S., Nair S., Govindan U., Arayambath S., et al., Effect of hybridization of organoclay with carbon black on the transport, mechanical, and adhesion properties of nanocomposites based on bromobutyl/epoxidized natural rubber blends, RSC Adv., 2016, 6, 33723-33732.
- [15] <http://www.chemicalize.org/structure/#!mol=epichlorohydrin>, Accessed 10 July 2015.
- [16] Arkles B., Hydrophobicity, Hydrophilicity and Silanes, Paint & Coatings Industry magazine, October 2006, 114-135.